PETROLEUM EXPLORATION AND DEVELOPMENT
Volume 50, Issue 1, February 2023
http://www.sciencedirect.com/journal/petroleum-exploration-and-development

Available online at www.sciencedirect.com
ScienceDirect

Cite this article as: PETROL. EXPLOR. DEVELOP., 2023, 50(1): 111–124.

RESEARCH PAPER

Differences of tuffaceous components dissolution and their impact on physical properties in sandstone reservoirs: A case study on Paleogene Wenchang Formation in Huizhou-Lufeng area, Zhu I Depression, Pearl River Mouth Basin, China

JIN Zihao[1], YUAN Guanghui[1, 2, *], ZHANG Xiangtao[3], CAO Yingchang[1, 2], DING Lin[3], LI Xiaoyan[3], FU Xiaohan[1]

1. Key Laboratory of Deep Oil and Gas, China University of Petroleum, Qingdao 266580, China;
2. Laboratory for Marine Mineral Resources, Qingdao National Laboratory for Marine Science and Technology, Qingdao 266071, China;
3. China National Offshore Oil Corporation Limited-Shenzhen, Shenzhen 518067, China

Abstract: The element geochemical characteristics and diagenetic alteration products of tuffaceous components in sandstone reservoirs of Paleogene Wenchang Formation in typical subsags of the Huizhou-Lufeng area of the Zhu I Depression, Pearl River Mouth Basin, were identified through microscopic analysis and quantitative analysis of main and trace elements. The impacts of dissolution of different tuffaceous components on physical properties of reservoirs were discussed through quantitative characterization of reservoir physical properties. The results show that there are mainly four types of tuffaceous components in the study area, which are acidic, intermediate, basic and alkaline tuffaceous components. The acidic tuffaceous components evolved in a process of strong alteration and weak dissolution of alteration products, with a large amount of kaolinite precipitated during alteration to disenable the improvement of porosity and permeability. The intermediate and alkaline tuffaceous components evolved in a process of strong dissolution of tuffaceous components and strong alteration of residual tuffaceous components; the dissolution of tuffaceous components created intergranular pores, but the alteration products such as autogenic quartz, apatite and illite deteriorated the pore structure; ultimately, the dissolution of tuffaceous components resulted in the increase of porosity but no increase of permeability of the reservoir. The basic tuffaceous components dominantly evolved in a process of dissolution of tuffaceous components to strong dissolution of alteration products; both tuffaceous components between particles and laumontite generated from alteration can be strongly dissolved to create pores; thus, the dissolution of tuffaceous components can significantly increase the physical properties of the reservoir.

Key words: Zhu I Depression; Huizhou Sag; Lufeng Sag; tuffaceous component; dissolution; physical property response; Paleogene Wenchang Formation

Introduction

Compared with an argillaceous matrix, a tuffaceous matrix is characterized by various types and complexities of components [1–6]. In addition, tuffaceous materials were prone to be dissolved during progressive burial diagenesis, which could increase porosity and provide material for the precipitation of authigenic minerals [4, 7–10]. Previous studies have shown that the genetic type, composition, and content of tuffaceous materials in clastic rocks can have different effects on the dissolution process [4–5]. Moreover, the dissolution of tuffaceous materials varies greatly in different burial stages and diagenetic environments [6–8], and has different influences on the development of pores in clastic reservoirs [9–11]. Therefore, the

Received date: 29 Apr. 2022; **Revised date:** 30 Dec. 2022.
*** Corresponding author.** E-mail: yuan.guanghui@upc.edu.cn
Foundation item: Supported by the China National Natural Science Foundation (41872140); Taishan Scholars and Young Experts Project (201909061); Qingdao Marine Science and Technology Pilot Special Fund for National Laboratory in Shandong Province (2021QNLM020001); Central University Innovation Fund (20CX06067A).
https://doi.org/10.1016/S1876-3804(22)60373-2

intensity of tuffaceous material dissolution and the mechanism of authigenic mineral precipitation determine whether the dissolution of tuffaceous materials can effectively improve the quality of the reservoir.

Volcanic events occurred frequently in the depositional period of the Eocene Wenchang Formation in Huizhou Sag and Lufeng Sag of the Pearl River Mouth Basin, and the genesis of tuff was complex with many varieties [9-12]. Previous studies have suggested that the dissolution of tuffaceous matrix in the reservoir of the study area could form secondary pores and improve the reservoir physical properties to some extent [9]. However, this understanding only considers the effect of tuffaceous dissolution on the reservoir space, and ignores the genetic relationship between authigenic minerals and tuffaceous alteration, as well as the changes of reservoir properties in the dissolution process of tuffaceous materials. In fact, the dissolution of tuffaceous components was common in the sandstone reservoirs from Member 6 to Member 3 of Wenchang Formation in Huizhou Sag and Lufeng Sag [9, 13], and many alteration products such as kaolinite, laumontite, and apatite can be found. Moreover, the dissolution intensity and the combination of alteration products vary with the types of tuffaceous materials. It is of great significance to systematically study the alteration pathways of tuffaceous materials and their porosity evolution to deepen the understanding of oil and gas reservoirs in the study area.

This work is focused mainly on the genetic relationship between authigenic minerals and dissolution of the tuffaceous materials in the sandstone reservoirs of the sixth to third members of the Paleogene Wenchang Formation in Huizhou Sag and Lufeng Sag of Zhu I Depression in the Pearl River Mouth Basin. It establishes the alteration pathways of different types of tuffaceous materials. Based on this, the change of reservoir physical properties in response to the tuffaceous dissolution are discussed to provide the basis for reservoir quality evaluation of tuffaceous sandstone reservoirs.

1. Geological background

The Huizhou Sag and Lufeng Sag are important hydrocarbon enrichment areas located in the eastern part of the Zhu I Depression in Pearl River Mouth Basin; they are distributed in the NEE direction and are divided by Huizhou-Lufeng low uplift [9, 13–19] (Fig. 1). The key layer for this study is the Wenchang Formation, which can be divided into six members from bottom to top (labeled Members 6, 5, 4, 3, 2, and 1 of the Wenchang Formation), corresponding to the initial, intense to shrinking periods of the complete basin rifting cycle [14, 18] (Fig. 1). Member 6 corresponds to the initial stage of basin rifting, during which the basin suffered uplift and denudation, accompanied by strong magmatic activity, and developed only a scattered

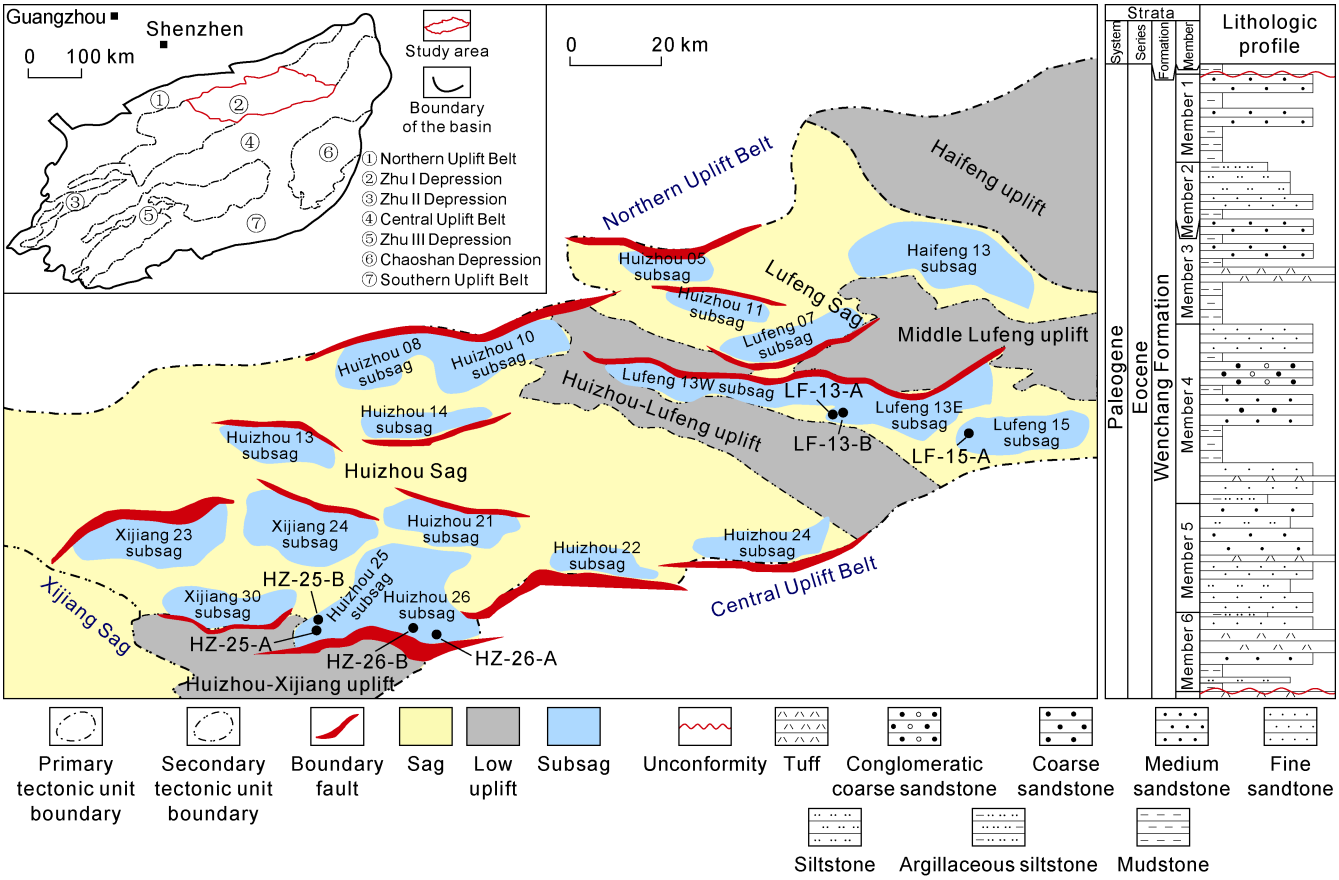

Fig. 1. Geologic map of the Huizhou Sag and Lufeng Sag in Pearl River Mouth Basin and comprehensive strata log diagram of Wenchang Formation [14–15].

small fan delta and braided river delta [13–14]. Members 5 and 4 correspond to the basin rifting expansion and intense period, with the rapid expansion of the lacustrine basin and the development of large braided river delta deposits [19–20]. Member 3 corresponds to the rifting transition period. Influenced by the Huizhou movement, basement uplift, and magmatic floor cleavage were widely developed, and strong uplift occurred in the Huizhou-Lufeng transition areas, accompanied by massive denudation of the Lower Member of the Wenchang Formation [14]. Members 2 and 1 correspond to the contraction and shrinking period of basin rifting, when the water in the lacustrine basin became shallower and the small braided river delta sediments were developed and dispersed again [13, 20]. In general, the sedimentary period of the Wenchang Formation was accompanied by multiple periods of volcanic activity. Due to the changes of intensity and periods of the volcanic activity and the different magmatic properties, the tuff matrixes in sandstone reservoirs of different subsags are of various types and have uneven contents [9, 12].

2. Samples and methods

The samples were taken from wells HZ-25-A and HZ-25-B in the Huizhou 25 subsag, wells HZ-26-A and HZ-26-B in the Huizhou 26 subsag, wells LF-13-A and LF-13-B in the Lufeng 13 subsag, and Well LF-15-A in the Lufeng 15 subsag (Fig. 1). The microscopic observation and quantitative statistics of porosity in thin sections were completed in the Key Laboratory of Deep Oil and Gas, China University of Petroleum (East China). The detection temperature in the laboratory was 23 °C and the relative humidity was 50%. A ZEISS AxTo Scope A1 APOL polarizing microscope, CL8200 MK5 cathode luminescence instrument, and ZEISS Crossbeam 550 double beam scanning electron microscope were used for the observations. The samples without dissolution of tuffaceous materials were selected to test the main components as well as trace substances in situ to determine the geochemical characteristics of the unaltered tuffaceous materials. For the samples with strong dissolution of tuffaceous materials, the characteristics of the tuffaceous material dissolution and the elementary composition of authigenic minerals were also determined. The main element analysis of the electron probe was performed in the Key Laboratory of Submarine Science and Exploration Technology of the Ministry of Education, Ocean University of China. The test voltage was 15 kV, the current was 20 nA, and the diameter of the test point was 5 μm. The in situ analysis of microzone trace elements was performed at the State Key Laboratory of Mineral Deposit Geochemistry, Institute of Geochemistry, Chinese Academy of Sciences. The equipment for element analysis included a GeoLasPro laser system and Agilent 7700x inductively coupled plasma mass spectrometer with a beam spot diameter of 50 μm.

3. Reservoir petrological characteristics

3.1. Detrital components

According to the observation of thin sections and the whole-bulk mineral compositions through X-ray diffraction analysis of 193 samples in the study area, significant differences were found in detrital components of the Wenchang Formation in different depressions (Fig. 2). The sandstone reservoirs in the Wenchang Formation of Huizhou Sag are mainly influenced by Mesozoic granites [13, 21], and are dominated by litharenite and feldspathic litharenite with a low content of quartz and high content of lithic and feldspar (Fig. 2a). The debris is composed mainly of granite and quartz lithic, and the feldspar is mainly potassium feldspar. The sandstone reservoir in Wenchang Formation of Lufeng Sag is influenced mainly by Mesozoic sediment provenance [22–23], and is

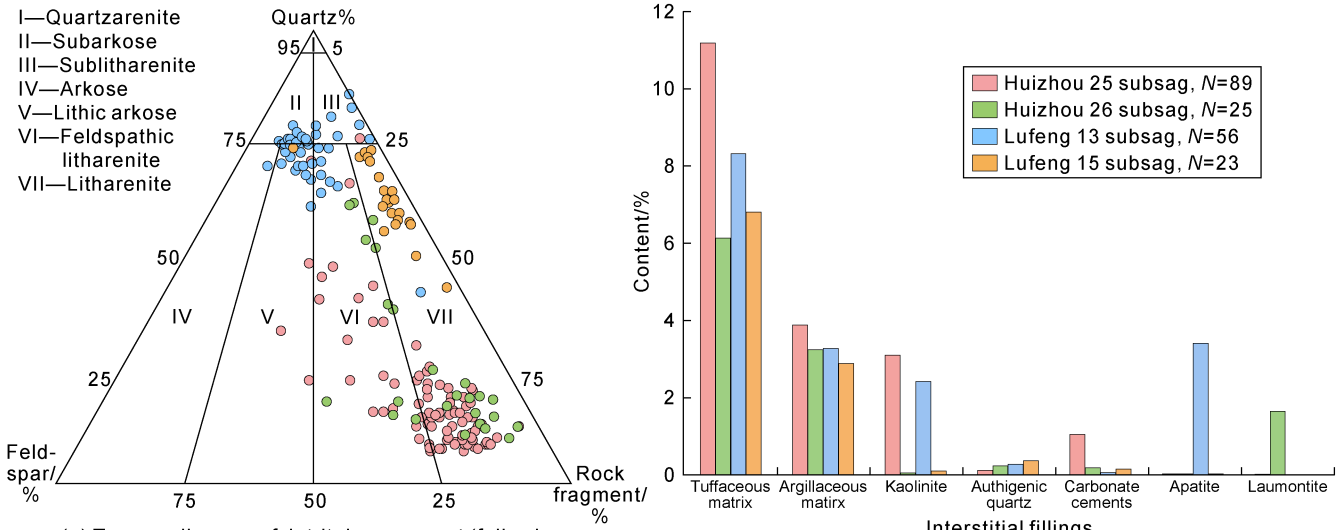

(a) Ternary diagram of detrital component (following the classification standard of reference 21)

(b) Bar chart of the average content of different types of interstitial fillings

Fig. 2. Ternary diagram of detrital components and bar chart of the average content of different types of interstitial fillings in Wenchang Formation of the study area.

composed mainly of subarkose, lithic arkose, sublitharenite, and litharenite with high content of quartz and low content of feldspar and lithic (Fig. 2a). The debris types are mainly quartzite and extrusive rock debris, and the feldspar is mainly potassium feldspar.

3.2. Interstitial fillings

According to the data gathered on thin sections and X-ray diffraction of clay minerals, the HZ25 subsag is dominated by a tuffaceous matrix averaging 11.19%, with an average content of clay matrix of 3.88%. The cementation is dominated by authigenic kaolinite and carbonate cements, with a small amount of authigenic quartz (Fig. 2b). The content of tuffaceous matrix in the HZ26 subsag is relatively low, with an average of 6.13%, with a clay matrix of 3.24%. The cementation is dominated by laumontite, with a small amount of authigenic quartz and carbonate cements (Fig. 2b). The average content of tuffaceous matrix and clay matrix in LF13 subsag is 8.33% and 3.27%, respectively (Fig. 2b). The content of tuffaceous matrix in Well LF-13-A is relatively high, and authigenic kaolinite, apatite and authigenic quartz are developed, while in Well LF-13-B the content of interstitial fillings in Well LF-13-B is generally low, mainly composed of authigenic quartz. The LF15 subsag is dominated by tuffaceous matrix with an average content of 6.79%, and the average amount of clay matrix is 2.88%. Authentic quartz is relatively well developed, with low content of the other types of cements (Fig. 2b).

3.3. Types and characteristics of tuffaceous materials

Compared with the clay matrix, the tuffaceous matrix has finer particle size and is often in the form of irregular clumps, without luminance under orthogonal light (Fig. 3a, 3b). The tuffaceous materials without obvious dissolution in the study area show intensive compaction, and only micropores with pore size less than 1 μm could be found (Fig. 3c). In the HZ25 subsag, the unaltered tuffaceous materials are glassy, and part of the tuffaceous materials show the characteristics of alteration caused by diagenetic fluid (Fig. 3a, 3b). It is brown-yellow under single polarized light, and has the characteristics of alteration products under orthogonal light (Fig. 3b). The unaltered tuffaceous materials in the HZ26 subsag are also glassy, but accompanied by the precipitation of iron minerals (Fig. 3d). The tuffaceous materials in LF15 and LF13 subsags have similar characteristics and are prone to be dissolved along the edge of the dissolution pore (Fig. 3e to 3h). It is difficult to classify the types of tuffaceous materials accurately based on observation of microscopic characteristics only. Therefore, the tuffaceous materials without obvious dissolution or alteration in each subsag were selected to compare their elementary compositions; the TAS discrimination diagram and the inactive trace element ratios (Zr/TiO_2 and Nb/Y) were used to classify the types of tuffaceous material [24–27] (Fig. 4). A total of 54 major-element data and 33 trace-element data were obtained (Table 1).

The tuffaceous materials in the HZ25 subsag are mainly distributed in the rhyolite-rhyodacite area, which indicates the source of acidic magma [25] (Fig. 4). They are characterized by a high content of silica and low content of alkalinity [25], with an average SiO_2 content of 67.93% and (Na_2O+K_2O) content of 3.38%, relatively rich in potassium (Table 1). The tuff in the HZ26 depression is mainly distributed in the trachyandesite-trachyte area,

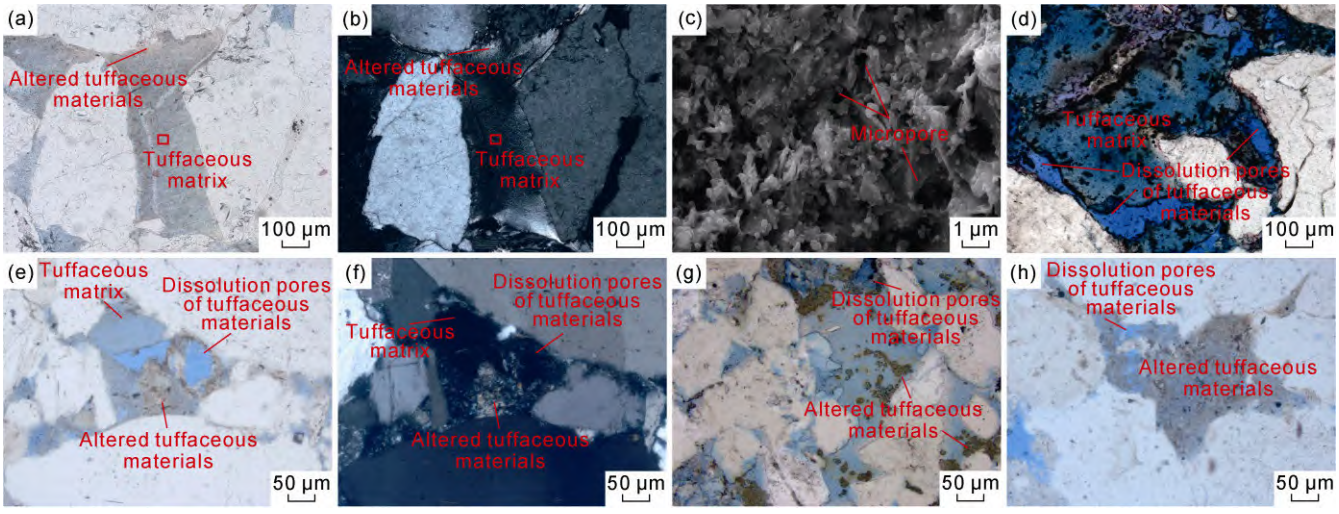

Fig. 3. Microscopic characteristics of tuffaceous matrix from Wenchang Formation in the study area. (a) Well HZ-25-B, 3775.52 m, WC6, tuffaceous matrix, with plane-polarized light. (b) Well HZ-25-B, 3775.52 m, WC6, tuffaceous matrix showing non-luminance under orthogonal light. (c) SEM (scanning electron microscope) feature in the red box in Fig. 3a-b, showing small micropores in the unaltered tuffaceous matix. (d) Well HZ-26-A, 3531.0 m, WC4, with the edge of the tuffaceous matrix dissolved with the precipitation of iron mineral, in plane-polarized light. (e) Well LF-13-B, 3455.3 m, WC3, brown altered tuffaceous matrix, with plane-polarized light. (f) Well LF-13-B, 3455.3 m, WC3, the tuff is photogenic under orthogonal light. (g) Well LF-13-A, 3413.0 m, WC3, the dispersion distribution of altered tuff, with plane-polarized light. (h) Well LF-15-A, 3645.4 m, WC4, the tuff was altered near the dissolution pores; with plane-polarized light.

which indicates the source of basic magma [25] (Fig. 4). It is characterized by low content of silica and high content of alkalinity, with an average SiO_2 content of 48.29% and (Na_2O+K_2O) content of 6.47%, relatively rich in sodium (Table 1). Tuffaceous materials in the LF15 and LF13 depressions are mainly distributed in the Andesite-Basaltic Andesite area, which indicates the intermediate magma source (Fig. 4), with an average SiO_2 content of 59.02% and (Na_2O+K_2O) content of 3.76%, relatively rich in potassium (Table 1). However, some tuff samples from well LF-13-A in the LF13 depression are distributed in partial alkalinity areas such as the trachyandesite and basaltic trachyandesite areas (Fig. 4), with an average SiO_2 content of 57.16% and (Na_2O+K_2O) content of 8.39%,

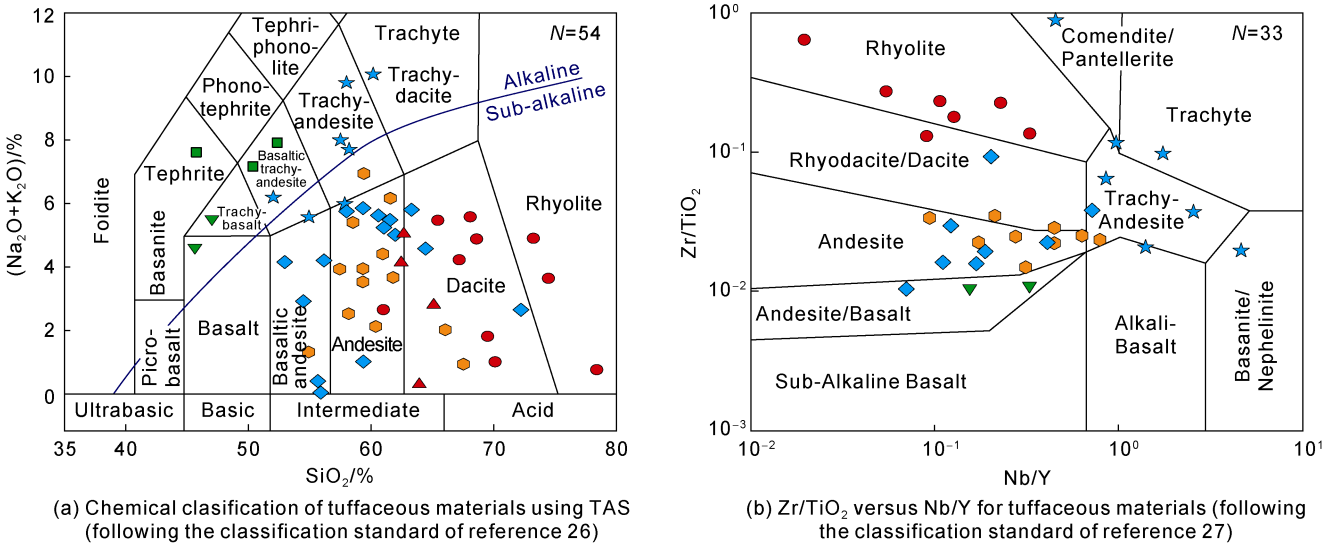

(a) Chemical clasification of tuffaceous materials using TAS (following the classification standard of reference 26)

(b) Zr/TiO_2 versus Nb/Y for tuffaceous materials (following the classification standard of reference 27)

Fig. 4. Classification of tuffaceous materials in Wenchang Formation of the study area.

Table 1. Composition of major elements and rare earth elements in unaltered tuffaceous materials of the Wenchang Formation in the study area

Major and trace elements	HZ25 subsag			HZ26 subsag			LF13 and LF15 subsags			LF13 subsag		
	Average/ %	Median/ %	Number of samples	Average/ %	Median/ %	Number of samples	Average/ %	Median/ %	Number of samples	Average/ %	Median/ %	Number of samples
SiO_2	67.93	68.07	14	48.29	47.33	5	59.02	59.38	30	57.16	57.97	5
Al_2O_3	21.45	23.60	14	16.68	15.98	5	18.28	19.16	30	13.59	14.03	5
Na_2O	0.27	0.23	14	3.48	4.07	5	0.73	0.11	30	8.08	7.40	5
MgO	1.02	0.70	14	1.43	1.69	5	1.05	0.84	30	1.61	1.59	5
K_2O	3.11	2.67	14	2.99	2.92	5	3.03	3.51	30	0.31	0.25	5
CaO	0.23	0.21	14	0.36	0.19	5	0.24	0.10	30	3.25	3.07	5
TiO_2	0.10	0.04	14	0.12	0.00	5	0.09	0.06	30	0.01	0.01	5
Cr_2O_3	0.01	0.00	14	0.03	0.01	5	0.01	0.01	30	0.00	0.00	5
MnO	0.02	0.01	14	0.02	0.02	5	0.09	0.02	30	0.02	0.03	5
FeO	1.48	0.88	14	1.36	1.20	5	2.58	1.01	30	2.58	2.82	5
P_2O_5	0.03	0.03	14	0.01	0.02	5	0.03	0.03	30	8.13	7.40	5
La	20.88	17.76	7	10.00	10.00	2	4.98	2.92	17	3.34	3.53	7
Ce	39.04	32.26	7	18.45	18.45	2	9.92	6.35	17	4.20	3.85	7
Pr	4.11	3.61	7	1.96	1.96	2	1.08	0.57	17	0.58	0.56	7
Nd	12.85	10.01	7	4.79	4.79	2	3.41	1.97	17	1.69	1.72	7
Sm	1.68	1.58	7	1.64	1.64	2	1.21	0.81	17	1.24	1.26	7
Eu	0.25	0.22	7	0.17	0.17	2	0.14	0.09	17	0.33	0.23	7
Gd	0.97	0.83	7	0.71	0.71	2	0.70	0.61	17	0.80	0.58	7
Tb	0.12	0.11	7	0.02	0.02	2	0.06	0.05	17	0.05	0.05	7
Dy	0.65	0.60	7	0.13	0.13	2	0.25	0.22	17	0.22	0.21	7
Ho	0.13	0.12	7	0.03	0.03	2	0.05	0.05	17	0.05	0.04	7
Er	0.38	0.31	7	0.10	0.10	2	0.16	0.15	17	0.18	0.16	7
Tm	0.06	0.05	7	0.03	0.03	2	0.02	0.02	17	0.02	0.02	7
Yb	0.40	0.31	7	0.10	0.10	2	0.12	0.10	17	0.16	0.13	7
Lu	0.07	0.06	7	0.04	0.04	2	0.02	0.01	17	0.02	0.02	7
∑REE	81.60	67.77	7	36.73	36.73	2	21.32	13.33	17	11.08	11.05	7
LREE/HREE	94.24	76.85	7	126.57	126.57	2	48.29	35.53	17	25.04	20.79	7
Eu/Eu*	0.92	0.91	7	0.91	0.91	2	0.85	0.81	17	0.88	0.85	7

relatively rich in sodium. The relatively high CaO and P_2O_5 contents, which average 3.25% and 8.13%, respectively (Table 1), also indicate the alkaline magma source.

4. Dissolution of tuffaceous materials

4.1. Dissolution pores formed by alteration of tuffaceous materials

The sandstone reservoirs in the Wenchang Formation of Huizhou Sag and Lufeng Sag are mainly in the middle diagenetic stage A1 to middle diagenetic stage A2, stages that were dominated by the dissolution of acidic fluids [9, 13, 28]. Previous studies have shown that the Eocene in Zhu I Depression experienced different degrees of uplift and denudation during the early sedimentary stage, which was the main period of meteoric water dissolution [13–14, 18]. Meanwhile, the concentration of atmospheric carbon dioxide was relatively high owing to intense volcanic eruptions [29], which provided stable acidic fluid for the dissolution of tuffaceous material in sandstone reservoirs of the Wenchang Formation. Later, in the deep burial process of Eocene, the infiltration depth of acidic meteoric water was limited, so it no longer acted on the reservoir to cause dissolution [13]. With an increase of burial depth and of temperature, organic acids generated by kerogen thermal evolution together with CO_2 generated by decarboxylation of organic acids entered the reservoir, providing the source of acidic fluid dissolution of tuffaceous materials [13, 30]. Microscopic characteristics show that there were relatively few dissolution pores developed in the acid tuffaceous materials in the HZ25 subsag, which were dominated by dissolution expansion along the edges of particles or tuffaceous micro-fractures (Fig. 5a). Also, it was hard to generate large-scale and effectively connected intergranular dissolution pores for the acid tuffaceous materials, and strong alteration often occurred near the dissolution pores (Fig. 5b). The dissolution of basic tuffaceous materials in the HZ26 subsag was relatively strong and the intergranular tuff dissolution pores were relatively developed with less residual tuffaceous materials (Fig. 5c, 5d). However, the dissolution pores in intermediate tuff in the LF15 subsag and Well LF-13-B were filled with a large amount of residual tuff (Fig. 5e, 5f). The alkaline tuffaceous materials in Well LF-13-A could be strongly dissolved to form intergranular dissolution pores, often accompanied by the precipitation of rod-like apatite or columnar apatite (Fig. 5g, 5h).

4.2. Characteristics of alteration products of tuffaceous materials

4.2.1. Authigenic clay minerals

The precipitation of authigenic clay minerals was closely related to dissolution of tuffaceous matrix. Taking authigenic kaolinite in the HZ25 subsag as an example, the kaolinite generated from alteration of tuff was generally in the form of small crystals (diameter less than 10 μm) and mostly precipitated at the edge between tuffaceous matrix and grains (Fig. 5b), or was in the form of agglomerate and wrapped by residual tuffaceous materials (Fig. 6a, 6b). Compared with the kaolinite generated from feldspar dissolution, the intercrystalline pores of kaolinite generated from tuff dissolution were not developed because the pores were filled with residual tuffaceous materials (Fig. 6b). In addition, the kaolinite generated from tuff dissolution and the residual tuff have

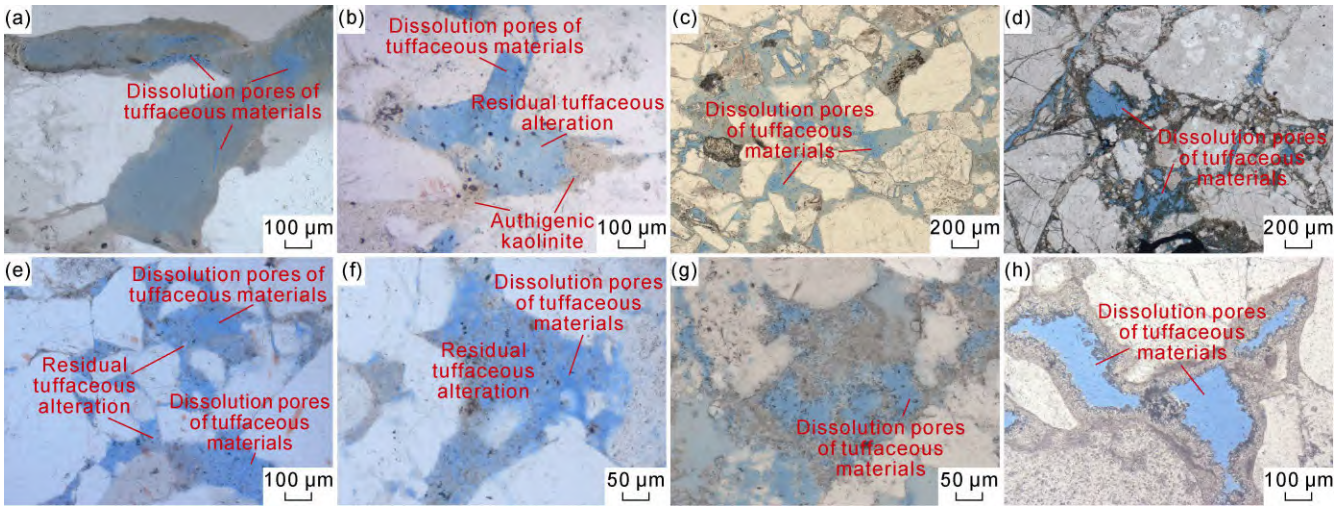

Fig. 5. Dissolution pores of different types of tuffaceous materials in the Wenchang Formation. (a) Well HZ-25-A, 3605 m, WC6, with acid tuffaceous dissolution pores, in plane-polarized light. (b) Well HZ-25-B, 3767.29 m, WC6, with acid-tuff dissolved along the edge of the grains and with deposited kaolinite, in plane-polarized light. (c) Well HZ-26-A, 3503.5 m, WC4, with dissolution pores in the basic-tuffaceous material, in plane-polarized light. (d) Well HZ-26-B, 3770 m, WC4, with less residual in the basic tuffaceous dissolution pores, in plane-polarized light. (e) Well LF-13-B, 3470 m, WC3 and (f) Well LF-13-B, 3470 m, WC3, with abundant residual in the intermediate tuffaceous dissolution pores, in plane-polarized light. (g) Well LF-13-A, 3413 m, WC3. (h) Well LF-13-A, 3451.5 m, WC3, with alkaline tuffaceous dissolution pores and the apatite precipitated at the edges of dissolution pores, in plane-polarized light.

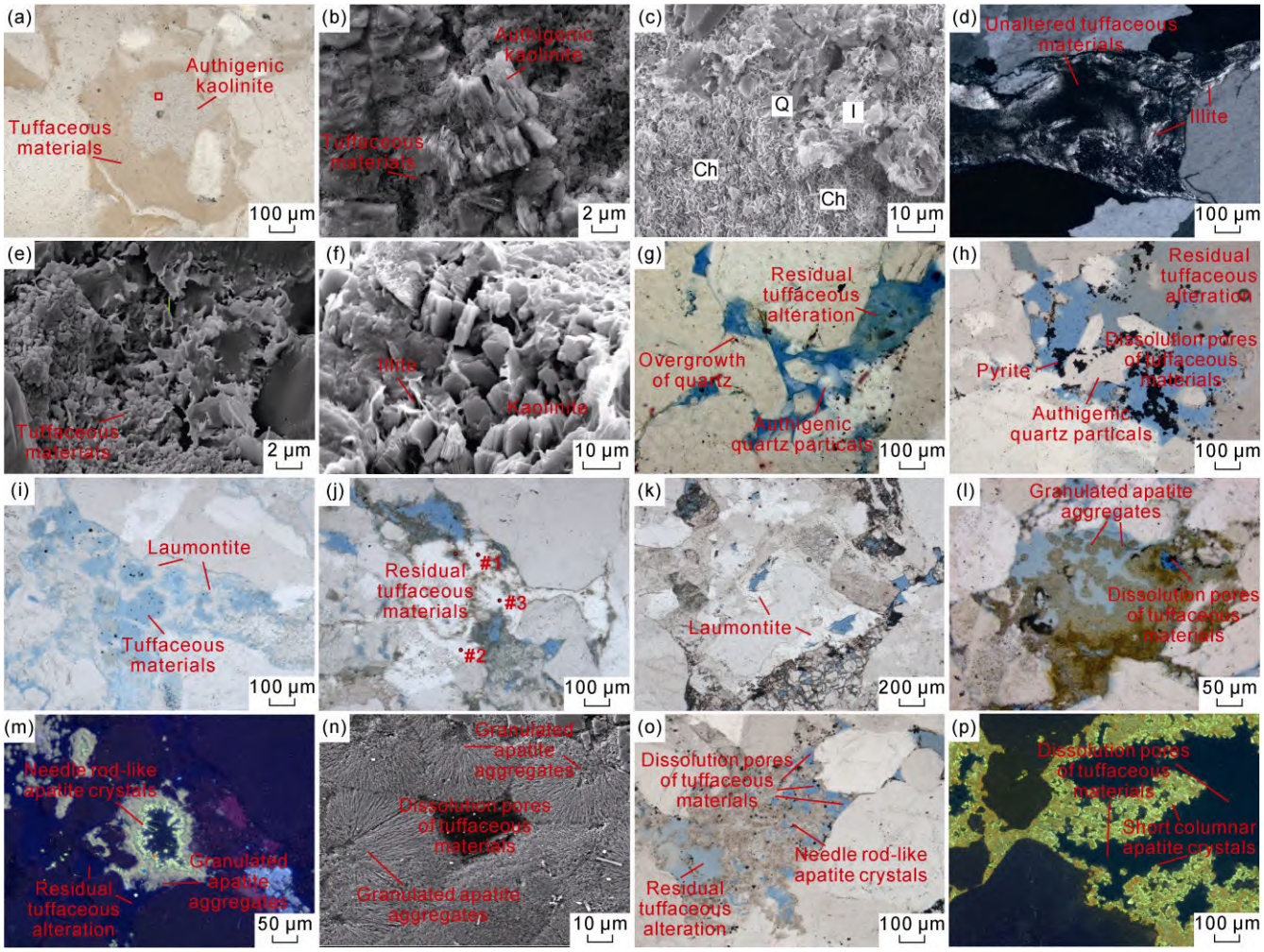

Fig. 6. Characteristics of alteration products of tuffaceous materials in the Wenchang Formation of the study area. (a) Well HZ-25-A, 3527.3 m, WC5, with acid-tuffaceous matter altered into kaolinite, in plane-polarized light. (b) SEM in the red box of Fig. 6(a), poor crystal shape of kaolinite was generated, intergranular pores were filled with tuffaceous matter, SEM. (c) Well HZ-26-A, 3415.2 m, WC4, basic-tuff altered into chlorite and illite, with the precipitation of authigenic quartz, SEM. (d) Well HZ-25-B, 3777.13 m, WC6, acid-tuff altered into illite along the edge of grains and microfracure, orthogonal light. (e) Well LF-15-A, 3710.9 m, WC4, intermediate tuff altered into illite, SEM. (f) Well LF-15-A, 3645.4 m, WC4, kaolinite. altered into illite, SEM; (g) Well LF-13-B, 3484 m, WC3, the intermediate tuff was dissolved and the pores were filled with authigenic quartz, in plane-polarized light. (h) Well LF-13-A, 3455 m, WC3, authigenic quartz precipitated in the tuffaceous dissolution pores, in plane-polarized light. (i) Well HZ-26-B, 3791 m, WC4. (j) Well HZ-26-B, 3816.5 m, WC4, laumontite precipitated in the basic tuffaceous dissolution pores with tuffaceous disslution residue, in plane-polarized light. (k) Well HZ-26-B, 3798 m, WC4, dissolution pores in the laumontite, in plane-polarized light. (l) Well LF-13-A, 3413 m, WC3, alkaline tuff altered into apatite, which was spherically formed along the edge of the grains or along the dissolved pores, in plane-polarized light. (m) Well LF-13-A, 3413 m, WC3, the early stage of apitite showed yellow-brown under cathode luminescence, while the late stage of apitite showed fluorescent green under cathode luminescence, CL (cathode luminescence). (n) Well LF-13-A, 3413 m, WC3, granulated apatite aggregates, SEM. (o) Well LF-13-A, 3430.6 m, WC3, needle rod-like apatite precipitated in the dissolution pores, intergranular pores filled with pyrite, in plane-polarized light. (p) Well LF-13-A, 3451.5 m, WC3, the core of the short columnar apatite showed orange-red under cathode luminescence, while the rim showed fluorescent green under cathode luminescence, CL.

similar distribution mode of rare earth elements (REE) (Fig. 7a), both of which have weak negative Eu anomalies (Table 1), with an average Eu/Eu* value of 0.92. Also, they have no homology with authigenic kaolinite near feldspar grains or dissolved feldspar (Fig. 7b). Chlorite was mostly associated with the alteration of basic tuffaceous matrix [5], and was developed mainly in the HZ26 subsag, accompanied by the precipitation of authigenic quartz microcrystals (Fig. 6c). Illite could be found in every subsag, the tuffaceous components being altered into illite between the edges along the particles (Fig. 6d, 6e). Additionally, the early-formed kaolinite and chlorite could be transformed into illite [31] (Fig. 6c, 6f).

4.2.2. Authigenic quartz

Authigenic quartz was widely developed in the reservoirs of the Wenchang Formation, and all types of tuffaceous dissolution can precipitate authigenic quartz. According to its crystallographic form, authigenic quartz can be divided into two types: microcrystalline quartz grains and the overgrowth of quartz (Fig. 6g, 6h). The overgrowth of quartz normally fills the tuffaceous disso-

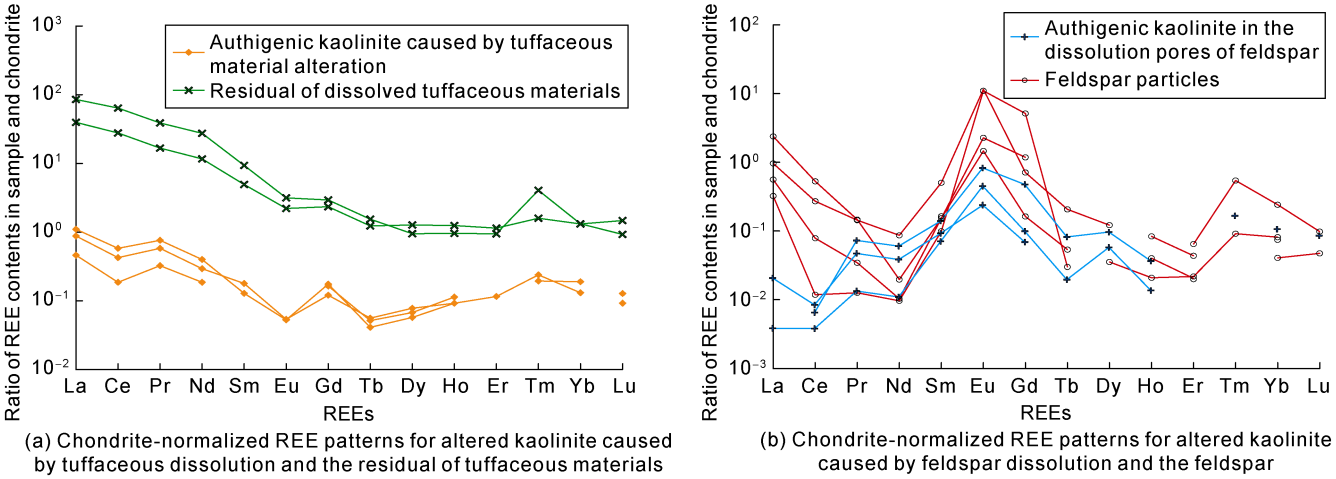

(a) Chondrite-normalized REE patterns for altered kaolinite caused by tuffaceous dissolution and the residual of tuffaceous materials

(b) Chondrite-normalized REE patterns for altered kaolinite caused by feldspar dissolution and the feldspar

Fig. 7. Distribution diagram of REE among different genetic types of kaolinite, feldspar and tuffaceous dissolution residue of Wenchang Formation.

lution pores or the nearby primary intergranular pores (Fig. 6g) with a usual thickness of 10–80 μm but up to 200 μm. The microcrystalline quartz consists usually of columnar dipyramid crystals, and the grains grow in random directions with different lengths (Fig. 6h). Compared with quartz particles, the principal elements such as Al and Fe are relatively enriched in the microcrystalline quartz grains and in the overgrowth of quartz (Fig. 8a). In addition, all the authigenic quartz retains a certain amount of light rare-earth elements (Fig. 8b), and all showed weak negative Eu anomalies (Table 1), which were distinctly different from the feldspar grains (Fig. 7b), suggesting that the authigenic quartz is more likely to be the alteration product of tuffaceous materials [32-33].

4.2.3. Laumontite

Previous studies have suggested that the precipitation of zeolite is closely related to the composition of the original material and that it was controlled by the chemical properties of formation liquid, among other factors [5, 34-35]. In the study area, the laumontite was commonly developed in the HZ26 subsag and was related to the dissolution of basic tuffaceous material. In addition, the laumontite could also be dissolved to different degrees to form dissolution pores (Fig. 6k). Compared with the residual tuffaceous alteration, the contents of SiO_2 and CaO were greater in the laumontite, while the contents of Al_2O_3 and K_2O were slightly less (Fig. 9). Furthermore, the contents of CaO in the residual tuffaceous alteration coated by the laumontite were somewhat lower than that of basic tuffaceous materials without alteration (Fig. 9). Therefore, the dissolution of basic tuffaceous matter can provide part of the calcium for the precipitation of laumontite [5, 25].

4.2.4. Apatite

Apatite developed only in the reservoir of Well LF-13-A

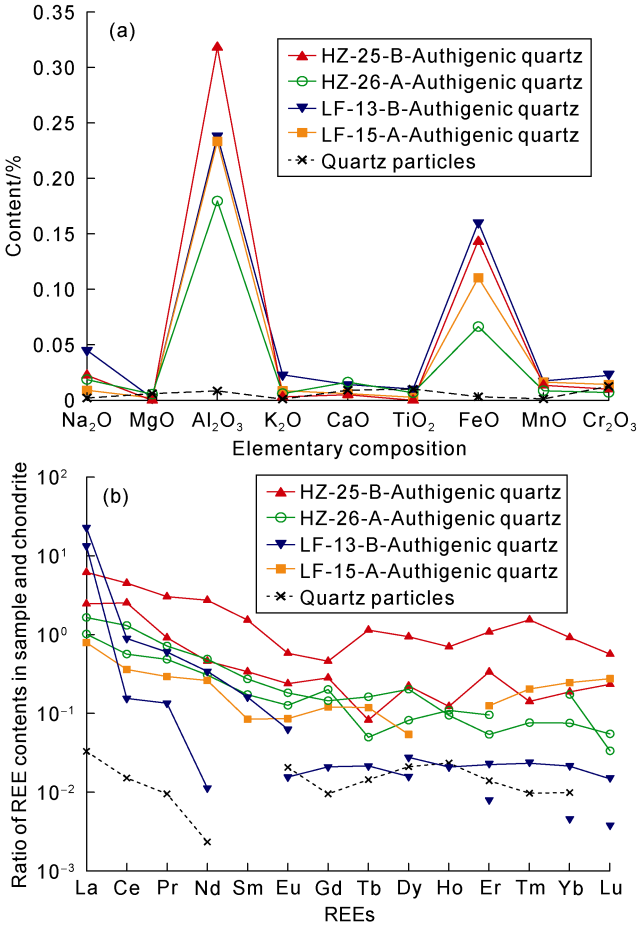

Fig. 8. Elemental geochemical characteristics of the authigenic quartz formed by tuffaceous alteration in Wenchang Formation. (a) The characteristics of the major elements (without Si) in the authigenic quartz formed by tuffaceous alteration. (b) The patterns of REE in the authigenic quartz formed by tuffaceous alteration.

in Wenchang Formation. According to its microscopic morphology and cathodic luminescence characteristics, the apatite can be divided into two stages: granulated apatite aggregates for the early stage and needle rod-like apatite and plate columnar apatite for the late stage (Fig.

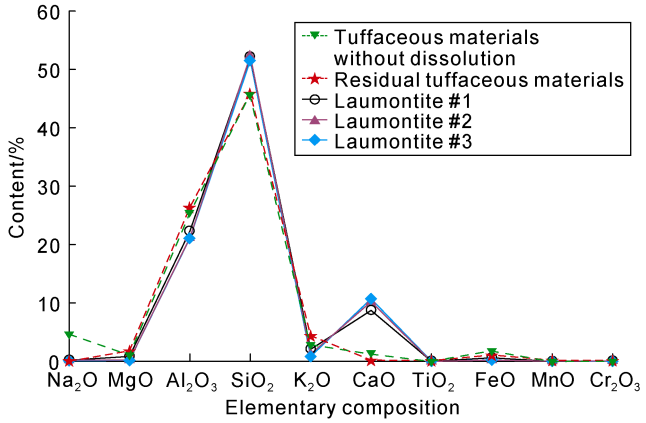

Fig. 9. Characteristics of the major elements in the laumontite formed by tuffaceous alteration in the Wenchang Formation (the test points are shown in Fig. 6j).

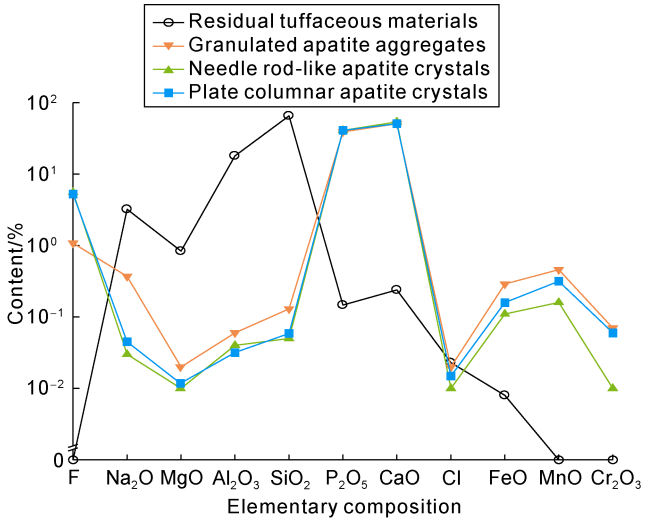

Fig. 10. Major elements of apatite caused by tuffaceous alteration of Wenchang Formation in the study area.

6l, 6p). The early stage of apatite was scattered in the alkaline tuffaceous matrix (Fig. 6l), or grew along the edges of the grains and the tuffaceous dissolution pores, and was yellow-brown under cathodic luminescence (Fig. 6m). The granulated apatite aggregates were composed of single crystals of fibrous or acicular apatite growing radially outward along the same growing core (Fig. 6n). At the rim of the granulated apatite aggregates, the late stage of needle rod-like apatite could be identified with fluorescent green color under cathodic luminescence (Fig. 6m). Some depths of the reservoirs showed strong dissolution of the tuffaceous material; the early stage of apatite did not develop. The apatite was dominated by needle rod-like apatite or plate columnar apatite (Fig. 6o, 6p), and the intercrystalline pores of apatite were filled with pyrite. The major-elements analysis showed that the contents of Ca and P in the residual tuffaceous materials were lower than those in the unaltered alkaline tuff (Fig. 10 and Table 1), indicating that the dissolution of alkaline tuff can provide material for the precipitation of apatite. In addition, the content of F was also an important index for the classification of apatite stages [36]. The content of F in the granulated apatite aggregate is relatively low, with an average content of 1.08%, while the contents in needle rod-like apatite and plate columnar apatite are 5.68% and 5.34%, respectively (Fig. 10). The absence of core or irregularity of core-rim in some plate columnar apatite also suggests that a different intensity of dissolution occurred in the early stage of apatite [37] (Fig. 6p).

4.3. Contents of tuffaceous dissolution and alteration products

In order to quantitatively characterize the relationship between dissolution of tuffaceous materials and alteration products of the Wenchang Formation in the study area, image analysis software was used to calculate the content of tuffaceous dissolution, the areal porosity of dissolution pores, and the contents of authigenic kaolinite, quartz, laumontite, and apatite for different types of tuffaceous material through thin sections (Fig. 11). Chlorite and illite are not discussed in this study because, due to their formation, they are difficult to calculate. With an increase of acid tuff dissolution, the content of authigenic kaolinite increases monotonically. The resulting areal porosity of the tuffaceous dissolution pores were generally less than 2%, and those contents were relatively high only in the zone with relatively low content of kaolinite (Fig. 11a). When the dissolution content of basic tuff was less than 4%, the authigenic mineral contents were relatively low, and intergranular dissolution pores developed. With an increase of the tuffaceous dissolution amount of basic tuff, the content of laumontite was positively correlated with the dissolution amount of basic tuff. However, due to the dissolution of laumontite, the contents of laumontite in some areas with high tuff dissolution content decreased (Fig. 11b). The intermediate tuff dissolution products were mainly authigenic quartz, which did not completely fill the dissolution pores, so the areal porosity of tuffaceous dissolution pores showed a positive correlation with the tuffaceous dissolution amount (Fig. 11c). There was also a positive correlation between the contents of apatite and the contents of alkaline tuff dissolution. Some apatite precipitated along the edge of the tuffaceous dissolution pores, leading to a significant increase of areal porosity of tuffaceous dissolution pores and the apatite contents in areas with high tuffaceous dissolution content (Fig. 11d).

5. Evolution of tuffaceous dissolution and its influence on the physical property of the reservoir

5.1. Evolution of tuffaceous dissolution

The intensity of tuffaceous dissolution and the differentiation of alteration products were controlled by the type and chemical properties of tuffaceous material [5, 9].

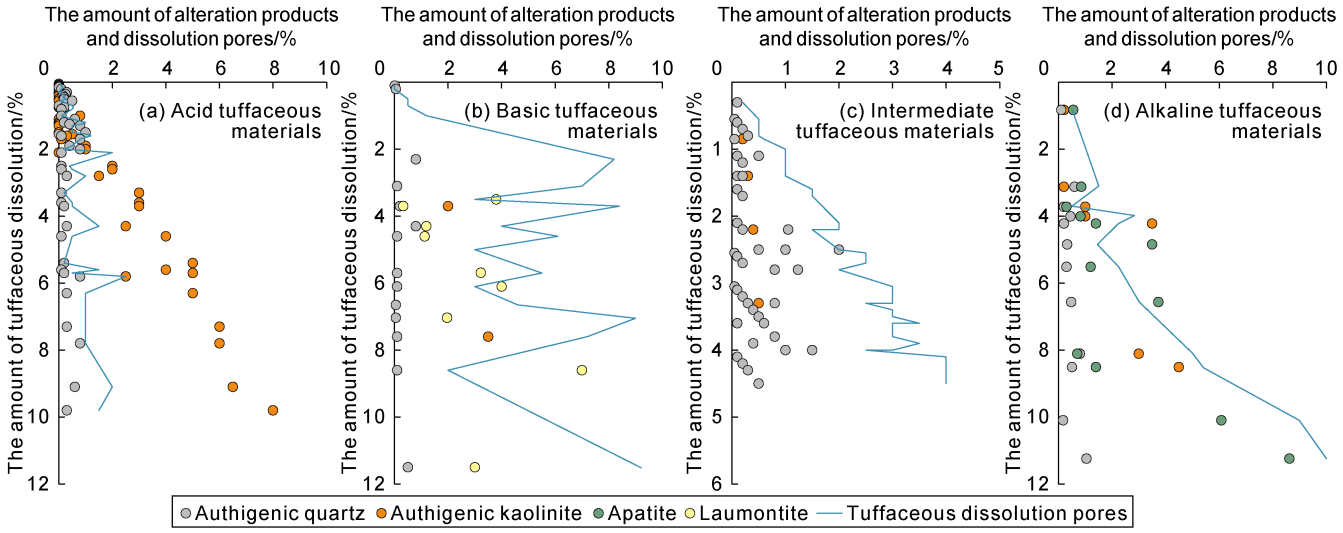

Fig. 11. Intersection diagram of the content of tuffaceous alteration and the content of alteration products and dissolution pores.

Combined with the diagenetic evolution of the reservoir in the study area, the evolution pathways of different types of tuffaceous dissolution were established (Fig. 12). Among them, weak dissolution showed itself in the acid tuff, mainly along the microfracture of tuff and along the rims of grains (Figs. 3a and 5a), and the tuffaceous dissolution pores were relatively isolated (Fig. 5a). In the process of dissolution, the tuff could be altered into kaolinite [5] (Figs. 6a, 6b, and 12) and precipitated microcrystalline quartz. With an increase of burial depth, the residual tuffaceous materials could change into illite (Figs. 6d and 12). The basic tuff was more likely to form tuffaceous dissolution pores [5, 9, 25] (Fig. 5c, 5d). With the dissolution of tuff, the residual tuff was changed into chlorite, with the precipitation of authigenic microcrystalline quartz (Figs. 6c and 12). In addition, plate-like or strip-like laumontite filled the dissolution pores of tuff (Fig. 6i), or appeared in the form of porous tight cementation (Figs. 6j and 12). With an increase of burial depth and of temperature, unstable minerals such as laumontite dissolved to form dissolution pores [4, 34] (Figs. 6k and 12), and the remnants of chlorite and intergranular tuffaceous dissolution were also changed into illite (Fig. 6e). The dissolution evolution pathways of intermediate tuff are similar to that of acidic tuff (Fig. 12), but the dissolution was stronger, the contents of alteration products were less, and the tuffaceous dissolution pores were relatively developed (Fig. 5e, 5f). Alkaline tuff was dissolved into pores by acidic fluid [24, 37] (Fig. 5g, 5h), and released active elements like Ca and P, resulting in the precipitation of early stages of granulated apatite aggregates and authigenic quartz along the edge of tuffaceous dissolution pores (Figs. 6h, 6m, 6o, and 12). With the continuous reaction of the fluid, the dissolution expansion of tuffaceous dissolution pores and the early stage of apatite occurred [37], and the needle rod-like late apatite were precipitated along the dissolution pores (Figs. 6m and 12). The alkaline tuff in some layers dissolved, and the tuffaceous dissolution residue underwent strong alteration with the precipitation of late-stage short columnar apatite crystals (Fig. 6p).

5.2. The response of tuffaceous material dissolution to physical property of the reservoir

The evolution pathways of dissolution of tuffaceous materials can be divided into three types, which have different effects on the physical properties of reservoirs.

(1) Type I is the evolution pathway with strong tuffaceous alteration, and weak dissolution of the alteration products. Taking acid tuff in the HZ25 subsag as an example: It does not readily dissolve or form effectively connected dissolution pores [5] (Fig. 5a, 5b). With increasing amounts of dissolution of tuffaceous material in the reservoir, abundant kaolinite was precipitated nearby (Fig. 11a). The tuffaceous dissolution pores were transformed into intercrystalline pores of kaolinite, and were compacted during burial evolution (Fig. 6a, 6b), which not only failed to improve the reservoir properties, but were also not conducive to the subsequent dissolution of acidic fluids [5, 31]. In addition, the kaolinite caused by alteration did not readily dissolve again, but plugged the pore throat because it would alter into illite [31] (Fig. 6d). Overall, in reservoirs bearing acid tuffaceous matters, the dissolution process of this material is dominated by strong alteration, and the precipitation of alteration products is not conducive to the improvement of reservoir physical properties.

(2) Type II follows an evolutionary pathway with strong dissolution of tuffaceous materials, and strong alteration of the residual. Taking intermediate tuff in Well LF-13-B and Well LF-15-A as examples, under the influence of acidic fluid, the intermediate tuffaceous materials

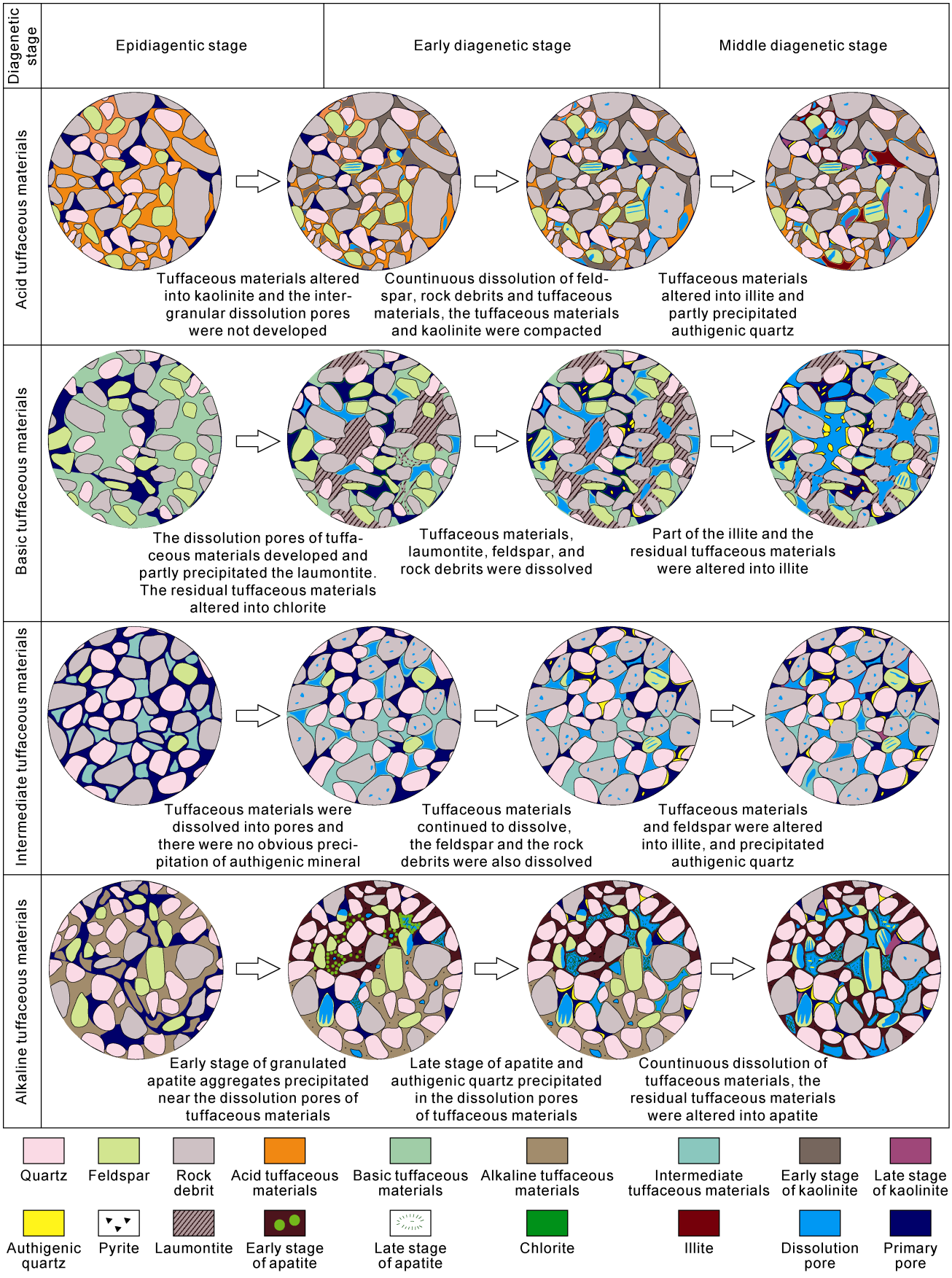

Fig. 12. Diagram of evolution pathways of tuffaceous dissolution.

dissolved and formed dissolution pores [5] (Figs. 3e and 5e). The dissolution byproducts in the reservoirs were mainly authigenic quartz in relatively small amounts (Figs. 6g and 11c); a large number of tuffaceous dissolu-

tion pores were still retained. However, due to the incomplete dissolution of tuffaceous material, the residual remained in the dissolution pores and was altered into illite (Figs. 5f, 6e and 6g), which led to the obstruction of pore-throat connectivity. The alkaline tuffaceous materials were also strongly dissolved in Well LF-13-A, where short columnar apatite crystals along the dissolution pores were precipitated (Figs. 5h and 6p) or, in the form of needle rod-like apatite crystals, filled the dissolution pores. Those apatite crystals braced each other like a frame (Figs. 5g and 6o), and could retain some tuffaceous dissolution pores, but it was not conducive to an increase of reservoir permeability. Therefore, although the tuffaceous dissolution caused by intermediate and alkaline tuff could effectively increase porosity, it was difficult to increase reservoir permeability.

(3) Type III is the evolution pathway with strong dissolution and alteration of tuffaceous material, and strong dissolution of the alteration products. In the reservoirs bearing basic tuffaceous materials in HZ26 subsag, the dissolution pores of tuffaceous materials were formed easily (Figs. 5c, 5d and 11b), and precipitated chlorite and laumontite (Fig. 6c, 6i–k). The precipitation of laumontite decreased the compaction in the burial process to some extent, and with the increase of burial depth, acidic fluid could dissolve laumontite again to form different scales of intergranular dissolution pores [4, 34] (Fig. 9k). Therefore, the dissolution of the basic tuffaceous material could not only form a large number of intergranular dissolution pores, but could also dissolve the alteration products again, which significantly improved the quality of the reservoir.

Combined with the physical characteristics of sandstone reservoirs in the Wenchang Formation of the study area, the tuffaceous dissolution pathway of Type III gives the most obvious improvement of reservoir physical properties. Observed mainly in the sandstone reservoirs in the HZ26 subsag with the enrichment of basic tuffaceous material, the average porosity is 14.88% and the average permeability is 24.63×10^{-3} μm² (Fig. 13 and Table 2). The dissolution of tuff and laumontite in the reservoirs provided fine pore throat connectivity.

The second best is the tuff dissolution pathway of Type II, which developed mainly in the LF13 subsag and LF15 subsag with the enrichment of intermediate or alkaline tuff in the reservoirs. The average porosity is 13.85%, and the average permeability is 2.69×10^{-3} μm² (Fig. 13 and Table 2). The intergranular tuff dissolution pores developed and were not fully filled by the authigenic minerals. Therefore, the dissolution of tuff could effectively connect the intergranular dissolution pores and primary pores to improve the quality of reservoirs. However, the permeability of the reservoir that underwent this type of tuff dissolution pathway is relatively low due to the blockage of pore throats by the residual of tuff dissolution, authigenic quartz, and apatite. Moreover, a large amount of authigenic kaolinite was deposited in the reservoir during burial evolution due to the tuff dissolution pathway of Type I. The alteration byproducts did not readily redissolve and the intergranular pores could be destroyed by the late compaction during the deep burial process. The reservoirs that underwent this kind of tuff dissolution could not significantly improve the reservoir physical properties; the average porosity is 11.37% and the average permeability is 4.13×10^{-3} μm² (Fig. 13 and Table 2).

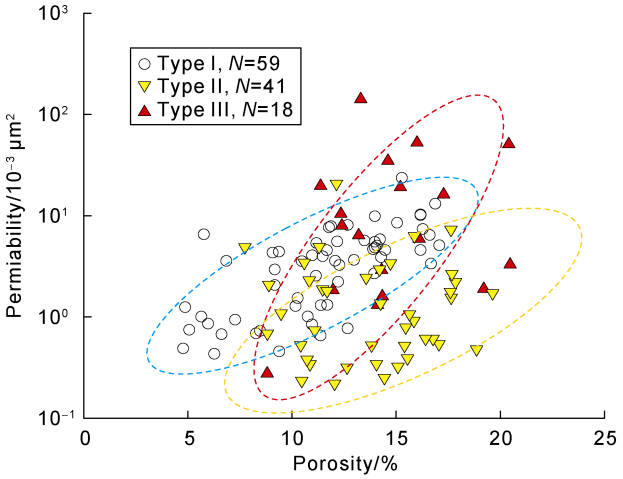

Fig. 13. Plot of the relationship between porosity and permeability of three types of tuff dissolution evolution pathways.

Table 2. Reservoir physical properties of each type of the evolution pathway of tuff dissolution

Dissolution type and evolution pathways	Representative Well	Types of tuff	Average content of tuff dissolution/%	Average porosity/ %	Average permeability/ 10^{-3} μm²	Main types of the pore
Type I, strong alteration, alteration products were difficult to dissolve	HZ-25-A, HZ-25-B	Acidic tuff	3.07	11.37	4.13	Tuff dissolution pores, intergranular pores of clay minerals, few feldspar dissolution pores;
Type II, strong dissolution, and strong alteration of the residual	LF-13-A, LF13-B, LF-15-A	Intermediate and alkaline tuff	2.62	13.85	2.69	Tuff dissolution pores, primary pores, intergranular pores of clay minerals and apatite crystals;
Type III, strong dissolution and alteration, and strong dissolution of the alteration products	HZ-26-A, HZ-26-B	Basic tuff	4.86	14.88	24.63	Tuff dissolution pores, laumontite dissolution pores, primary pores, intergranular pores of clay minerals.

6. Conclusions

There were four main types of tuffaceous matrix developed in the sandstone reservoirs in the Wenchang Formation of Huizhou Sag and Lufeng sag. They were acid, intermediate, basic, and alkaline tuffaceous materials. The type of tuffaceous matrix determined the ability to form dissolution pores and alteration products, which was the fundamental reason for the differential dissolution evolution of tuffaceous materials. The acid tuffaceous material did not readily dissolve into pores, and was transformed mainly into authigenic kaolinite and illite. The intermediate tuffaceous material was unstable in the burial diagenesis, and it easily formed dissolution pores. The authigenic quartz precipitated, and the residual of intergranular tuffaceous materials was transformed to clay minerals. The dissolution pores were easily formed in the basic tuffaceous material, and the residual tuffaceous materials changed into chlorite. The basic tuffaceous materials could also be transformed into laumontite in some of the reservoirs, which provided the material for later dissolution. The alkaline tuffaceous materials tended to be altered alone in the tuffaceous dissolution pores and precipitated apatite. With the expansion of the dissolution of tuffaceous dissolution pores, the late stage of authigenic apatite crystals with more regular crystal shape were precipitated at the edge of the dissolution pore.

According to the dissolution evolution pathways and the amount of alteration products of different types of tuffaceous material in each subsag, the dissolution of tuffaceous materials can be divided into three types, which had different effects on the physical properties of the reservoir. The most constructive for the physical properties of the reservoir was the dissolution of basic tuffaceous materials, which experienced an evolutionary pathway of both strong dissolution of tuffaceous materials and the alteration products. The reservoir spaces were dominated by intergranular pores with the best pore throat structure. Therefore, the dissolution of this kind of tuffaceous materials can effectively improve the porosity and permeability of the reservoir. The second was the dissolution of intermediate and alkaline tuffaceous materials, which was the evolutionary pathway of strong dissolution of tuffaceous materials and strong alteration of the residual tuffaceous materials. The reservoir spaces were dominated by dissolved intergranular pores and primary intergranular pores, but alteration products such as quartz, illite, and apatite would block the pore throats to some extent. Overall, the tuffaceous dissolution showed increasing porosity and reduction of permeability in the reservoirs. The evolution pathway of strong alteration of tuffaceous materials and the undissolved alteration products was dominated by the dissolution of acid tuffaceous materials. The reservoir spaces were dominated by the altered kaolinite with undeveloped intercrystalline pores, which was not conducive to the improvement of quality of the reservoirs.

References

[1] MARSAGLIA K M, BARONE M, CRITELLI S, et al. Petrography of volcaniclastic rocks in intra-arc volcano-bounded to fault-bounded basins of the Rosario segment of the Lower Cretaceous Alisitos oceanic arc, Baja California, Mexico. Sedimentary Geology, 2016, 336: 138–146.

[2] PENG Hao, YIN Cheng, HE Qinglin, et al. Development characteristics and petroleum geological significance of Permian pyroclastic flow volcanic rocks in Western Sichuan Basin, SW China. Petroleum Exploration and Development, 2022, 49(1): 56–67.

[3] LIU Ran, LUO Bing, LI Ya, et al. Relationship between Permian volcanic rocks distribution and karst paleogeomorphology of Maokou Formation and its significance for petroleum exploration in western Sichuan Basin, SW China. Petroleum Exploration and Development, 2021, 48(3): 575–585.

[4] ZHU Shifa, ZHU Xiaomin, LIU Xuechao, et al. Alteration products of volcanic materials and their influence on reservoir space in hydrocarbon reservoirs: Evidence from Lower Permian strata in Ke-Xia region, Junggar Basin. Acta Petrolei Sinica, 2014, 35(2): 276–285.

[5] WANG Hongyu, FAN Tailiang, XIAO Yingying, et al. Effect of tuffaceous components on physical property of sandstone reservoir. Acta Petrolei Sinica, 2010, 31(3): 432–439.

[6] WEI W, ZHU X M, KAREM A, et al. Depositional and compositional controls on diagenesis of the mixed siliciclastic-volcaniclastic sandstones: A case study of the Lower Cretaceous in Erennaoer Sag, Erlian Basin, NE China. Journal of Petroleum Science and Engineering, 2020, 188: 106855.

[7] WANG Jian, ZHOU Lu, LIU Jin, et al. Acid-base alternation diagenesis and its influence on shale reservoirs in the Permian Lucaogou Formation, Jimusar Sag, Junggar Basin, NW China. Petroleum Exploration and Development, 2020, 47(5): 898–912.

[8] YAO W J, CHEN Z H, DONG X M, et al. Storage space, pore–throat structure of igneous rocks and the significance to petroleum accumulation: An example from Junggar Basin, western China. Marine and Petroleum Geology, 2021, 133: 105270.

[9] TIAN Lixin. Genesis mechanism of tuffaceous materials in Paleogene large-scale glutenite reservoirs and implications for hydrocarbon exploration in the Huizhou Depression, Pearl River Mouth Basin. Earth Science, 2022, 47(2): 452–463.

[10] ZHANG Chenglin, ZHANG Jian, WU Jianfa, et al. Summary and discussion on tuffaceous reservoir research progress. Fault-Block Oil & Gas Field, 2016, 23(5): 545–548.

[11] LENG Jie, LIU Jie, CHEN Anqing, et al. Genesis of Mesozoic intermediate-basic volcanic reservoirs in Hui-

Huizhou 26-6 buried hill, Pearl River Mouth Basin, China. Journal of Chengdu University of Technology (Science & Technology Edition), 2021, 48(6): 661–674.

[12] ZHANG Bin, WANG Pujun, ZHANG Gongcheng, et al. Cenozoic volcanic rocks in the Pearl River Mouth and Southeast Hainan Basins of South China Sea and their implications for petroleum geology. Petroleum Exploration and Development, 2013, 40(6): 657–665.

[13] DING Lin, LI Xiaoyan, ZHOU Fengjuan, et al. Differential development characteristics and main controlling factors of the Paleogene high-quality reservoirs from the Zhu I Depression in the Pearl River Mouth Basin: A case on Wenchang Formation at Lufeng area and Huizhou area. Acta Petrologica et Mineralogica, 2022, 41(1): 75–86.

[14] SHI Hesheng, DU Jiayuan, MEI Lianfu, et al. Huizhou Movement and its significance in Pearl River Mouth Basin, China. Petroleum Exploration and Development, 2020, 47(3): 447–461.

[15] ZHAO Q, ZHU H T, ZHANG X T, et al. Geomorphologic reconstruction of an uplift in a continental basin with a source-to-sink balance: An example from the Huizhou-Lufeng Uplift, Pearl River Mouth Basin, South China Sea. Marine and Petroleum Geology, 2021, 128: 104984.

[16] TIAN Lixin. Sedimentary-reservoir characteristics under control of transfer model and implications for hydrocarbon exploration in Huizhou Depression, Pearl River Mouth Basin. Earth Science, 2021, 46(11): 4043–4056.

[17] WANG X D, ZHANG X T, LIN H M, et al. Paleogene geological framework and tectonic evolution of the central anticlinal zone in Lufeng 13 Sag, Pearl River Mouth Basin. Petroleum Research, 2019, 4(3): 238–249.

[18] ZHANG Xiangtao, LIU Pei, WANG Wenyong, et al. Controlling effect of tectonic transformation in Paleogene Wenchang Formation on oil and gas accumulation in Zhu I Depression. Earth Science, 2021, 46(5): 1797–1813.

[19] MI Lijun, ZHANG Xiangtao, WANG Xudong, et al. Tectonic and sedimentary differences of Paleogene and their control on hydrocarbon accumulation in Lufeng Sag, Pearl River Mouth Basin. China Offshore Oil and Gas, 2018, 30(5): 1–10.

[20] ZHENG Jinyun, GAO Yangdong, ZHANG Xiangtao, et al. Tectonic evolution cycles and Cenozoic sedimentary environment changes in the Pearl River Mouth Basin. Earth Science, 2022, 47(7): 2374–2390.

[21] FORK R L, ANDREWS P B, LEWIS D W. Detrital sedimentary rock classification and nomenclature for use in New Zealand. New Zealand Journal of Geology and Geophysics, 1970, 13: 937–968.

[22] ZHOU Fengjuan, DING Lin, MA Yongkun, et al. Detrital zircon U-Pb age characteristics of Wenchang Formation in Lufeng 13 eastern Sag and its significance for provenance tracing. China Offshore Oil and Gas, 2020, 32(4): 46–55.

[23] WAN Qionghua, LIU Weixin, LUO Wei, et al. Reservoir quality differences and major factors controlling low-permeability reservoirs of Oilfield A in the Lufeng Sag, Pearl River Mouth Basin. Oil & Gas Geology, 2017, 38(3): 551–560.

[24] LAWRENCE L, SPANDLER C, ROBERTS E M, et al. Mineralogy and origin of the alkaline Nsungwe Formation tuffs of the Rukwa Rift Basin, southwestern Tanzania. Lithos, 2021, 380-381: 105885.

[25] CICERALI D, ARSLAN M, ABDIOGLU Y E, et al. Mineralogy, chemistry, and genesis of zeolitization in Eocene tuffs from the Bayburt area (NE Turkey): Constraints on alteration processes of acidic pyroclastic deposits. Journal of African Earth Sciences, 2020, 162: 103690.

[26] LE MAITRE, R W. A classification of igneous rocks and glossary of terms. Oxford: Blackwell Science Publication, 1989: 193.

[27] WINCHESTER J A, FLOYD P A. 1977. Geochemical discrimination of different magna series and their differentiation products using immobile elements. Chemical Geology, 1997, 20: 325–343.

[28] GE Jiawang, ZHU Xiaomin, PAN Rong, et al. A quantitative porosity evolution model of sandstone for Wenchang Formation in Huizhou Depression, Pearl River Mouth Basin: A case study for braided fluvial delta reservoir of HZ-A area. Acta Sedimentologica Sinica, 2015, 33(1): 183–193.

[29] GUO Z, WILSON M, DINGWELL D B, et al. India-Asia collision as a driver of atmospheric CO_2 in the Cenozoic. Nature Communications, 2021, 12(1): 3891–3911.

[30] LONG Gengsheng, SHI Hesheng, ZHENG Rongcai, et al. Diagenesis and porosity evolution of deep reservoirs in Huizhou Depression, Pearl River Mouth basin. Acta Petrologica et Mineralogica, 2011, 30(4): 665–673.

[31] YUAN Guanghui, CAO Yingchang, XI Kelai, et al. Feldspar dissolution and its impact on physical properties of Paleogene clastic reservoirs in the northern slope zone of the Dongying Sag. Acta Petrolei Sinica, 2013, 34(5): 853–866.

[32] LAWRENCE M G, GREIG A, COLLERSON K D, et al. Rare earth element and yttrium variability in South East Queensland waterways. Aquatic Geochemistry, 2006, 12(1): 39–72.

[33] WANG Y Z, FU Y H, CAO Y C, et al. Sources of authigenic quartz in the Permian tight sandstones close to Gaoqing Fault, Dongying Sag, Bohai Bay Basin, China. Marine and Petroleum Geology, 2020, 113: 104109.

[34] WANG Tao, ZHANG Shengyin, WEI Pu, et al. Genesis of zeolite minerals and its influences on reservoir properties. Lithologic Reservoirs, 2022, 34(1): 175–186.

[35] VANIMAN D T, CHIPERA S J, BISH D L, et al. Quantification of unsaturated-zone alteration and cation exchange in zeolitized tuffs at Yucca Mountain, Nevada, USA. Geochimica et Cosmochimica Acta, 2001, 65(20): 3409–3433.

[36] AUBINEAU J, PARAT F, ELGHALI A, et al. Highly variable content of fluorapatite-hosted CO_3^{2-} in the Upper Cretaceous/Paleogene phosphorites (Morocco) and implications for paleodepositional conditions. Chemical Geology, 2022, 597: 120818.

[37] SEPIDBAR F, GHORBANI G, SIMON A C, et al. Formation of the Chah-Gaz iron oxide-apatite ore (IOA) deposit, Bafq District, Iran: Constraints from halogens, trace element concentrations, and Sr-Nd isotopes of fluorapatite. Ore Geology Reviews, 2022, 140: 104599.